BALLISTIC LIMIT PERFORMANCE OF BI-LAYER CERAMIC/METAL COMPOSITE ARMOUR UNDER RADIAL CONFINING PRESSURE

JIAQI DAI[1] & SUWEN CHEN[1,2]
[1]College of Civil Engineering, Tongji University, China
[2]State Key Laboratory of Disaster Reduction in Civil Engineering, Tongji University, China

ABSTRACT

The bi-layer armour composed of a front ceramic plate and a metal backplate is a typical composite protective structure. The ceramic serves to erode the projectile. Ceramics are sensitive to multi-axial stress states. To investigate the anti-penetration performance under confining pressure, a verified SPH–FEM numerical simulation model was established. The penetration experiments under higher confining pressures were conducted. Two parameters, the maximum biaxial confining pressure and the confining pressure ratio, were introduced to evaluate the prestress state of the ceramic. Finally, based on experimental and simulation results, a ballistic limit velocity calculation method and a fast computation formula considering the confining pressure were proposed. The validity of the proposed formula was verified through comparison of results from physical experiments and numerical simulations. This research provided significant insights for further research on the anti-penetration performance of ceramic/metal composite armour.

Keywords: ballistic performance, ceramic composite armour, ballistic limit velocity, energy dissipation.

1 INTRODUCTION

Ceramics are utilized on the impact face of armour protection due to the low density and high hardness. The metal backing plate attached to the ceramic front plate can inhibit the bending and cracking of ceramics under impact. The bi-layer ceramic/metal composite armour has been demonstrated to be a cost-effective protective structure.

Ceramics have a compressive strength of 10^0–10^1 GPa, while the tensile strength is only about 10% of the compressive strength. To overcome the significant difference between tensile and compressive strengths of ceramics, pre-compressive stress is introduced. Prestress ceramics can be categorized into three types based on applied prestress: hydrostatic prestress, radial prestress and axial prestress. Due to the difficulty of physical realization of hydrostatic prestress, radial and axial prestressing of ceramics has become the main approach for studying the anti-penetration performance of prestressed ceramics. Experiment and simulation on the anti-penetration performance of ceramic composite armour under confinement and prestress were performed in Sherman [1] and Holmquist and Johnson [2]. Results showed that both hydrostatic prestress and radial prestress can improve the ballistic performance of composite armour at the same level, while the enhancement of axial prestress was limited. In Farbaniec et al. [3], microstructural observations revealed the different impact failure modes between axial prestress and radial prestress ceramics, which demonstrated that radial prestress was more effective in improving impact resistance. Long rod projectile experiments on radial constrained ceramic armour were conducted in Chi et al. [4], Lundberg et al. [5] and Xu et al. [6], showing that radial prestress can extend the dwell time, thereby increasing the erosion of the projectile.

The anti-penetration performance of composite armour is evaluated through the ballistic limit velocity. This represents the initial velocity of a test projectile that just penetrates a specific type of composite armour. In research on non-prestress ceramic composite armour,

WIT Transactions on The Built Environment, Vol 215,
www.witpress.com, ISSN 1743-3509 (on-line)
doi:10.2495/SUSI250111

empirical formulas [7], [8] or theoretical analytical models [9]–[11] for calculating the ballistic limit velocity were developed. Based on existing researches, ballistic limit tests of prestress ceramics were carried out in Zhang et al. [12], [13], which indicated that radial prestress can significantly enhance the ballistic limit velocity of ceramic/metal composite armour. Prestress with 10^2 MPa level increased the ballistic limit velocity by approximately 30%.

In summary, there are still the following issues on the ballistic limit velocity of ceramic composite armour under radial prestress: there is no clear indicator for measuring the prestress level of different ceramics, and the theoretical calculation method for ballistic limit velocity under radial prestress is lacking. This paper presents the following research: a prestress ratio is proposed to measure the ceramic prestress level, a calculation method for the compressive, tensile, and shear strength of ceramics under radial prestress is established based on the JH-2 constitutive model, a method for calculating the ballistic limit velocity of prestress ceramic composite armour is derived based on the energy balance principle.

2 ANALYTIC MODEL BASED ON THE PRINCIPLE OF ENERGY DISSIPATION

The principle of energy dissipation is a commonly used method in theoretical research on ballistic performance. This method has the following two main advantages: (1) a clear physical meaning; and (2) avoidance of the dynamic analysis of the penetration process, directly obtaining the state parameters of the projectile at the ballistic terminal.

This section first introduces how to determine the strength of ceramics under confining pressure using the JH-2 constitutive model. Subsequently, an energy dissipation formula for the armour system is established considering the strength enhancement. Finally, the ballistic performance of composite armour is derived.

2.1 Determination of ceramic strength under confining pressure

The JH-2 constitutive model [14] is widely used to describe the mechanical behaviour of brittle geomaterials, ceramics, and glass under dynamic conditions. The strength surface is characterized by hydrostatic pressure and equivalent stress. As shown in Fig. 1, the loading curve under uniaxial loading is a straight line passing through the origin with a slope of 3. Similarly, under biaxial loading conditions, the loading curve has a slope of 1.5. The intersection points of the uniaxial and biaxial loading curves with the strength surface of the JH-2 model represent the uniaxial compressive strength of the material and the maximum radial confining pressure, respectively.

Eqn (1.1) presents the stress tensor of ceramics when reaching the normal strength $\sigma_{\mathrm{c,c/c,t}}$ in the third direction under radial confining pressure. Compression is considered positive in the equation. The equivalent stress and hydrostatic pressure for this stress state can be obtained from the stress tensor, as shown in eqn (1.2). Substituting these into the strength surface equation of the JH-2 constitutive model allows solving for the strength in the third direction. eqn (1.3) has two solutions with opposite signs, corresponding to the compressive strength and tensile strength under a confining pressure of P_{conf}. The tensor given in eqn (2) is used to solve for the shear strength $\tau_{\mathrm{c,s}}$ under confining pressure.

$$\boldsymbol{\sigma} = \begin{bmatrix} P_{\mathrm{conf}} & & \\ & P_{\mathrm{conf}} & \\ & & \sigma_{\mathrm{c,c/c,t}} \end{bmatrix}, \tag{1.1}$$

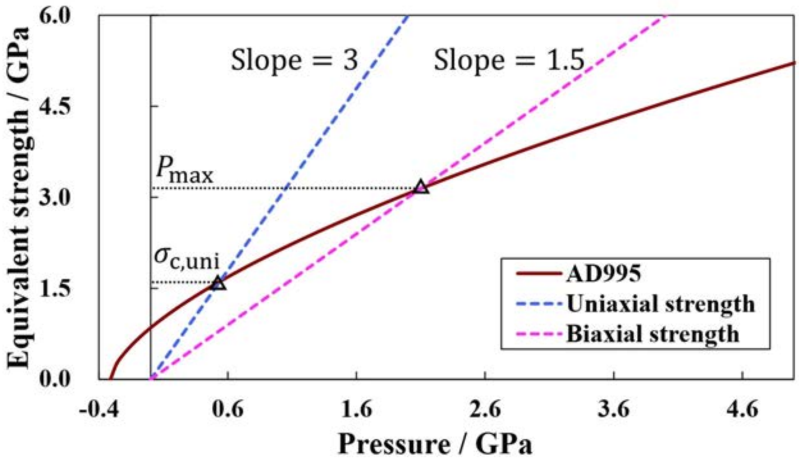

Figure 1: Determination of uniaxial and biaxial compressive strength of AD995 ceramics based on JH-2 constitutive model.

$$\begin{cases} \sigma^* = \sqrt{\left(P_{\mathrm{conf}} - \sigma_{\mathrm{c,c/c,t}}\right)^2} \\ P^* = \frac{1}{3}\left(2P_{\mathrm{conf}} + \sigma_{\mathrm{c,c/c,t}}\right) \end{cases}, \tag{1.2}$$

$$\frac{\sigma^*}{\sigma_{\mathrm{HEL}}} = A\left(\frac{P^*+T}{P_{\mathrm{HEL}}}\right)^N. \tag{1.3}$$

$$\boldsymbol{\sigma} = \begin{bmatrix} P_{\mathrm{conf}} & & \tau_{\mathrm{c,s}} \\ & P_{\mathrm{conf}} & \\ \tau_{\mathrm{c,s}} & & \end{bmatrix}. \tag{2}$$

- P_{conf} is the confining pressure.
- $\sigma_{\mathrm{c,c/c,t}}$ is the normal strength of ceramic.
- A and N are JH-2 parameter.
- σ_{HEL}, P_{HEL} and T are Hugoniot strength, hydrostatic pressure at Hugoniot stress and hydrostatic tensile strength.

Fig. 2 shows the variation of the compressive strength of AD995 ceramics with the confining pressure ratio. The results indicate that the compressive strength of the ceramic increases monotonically with the confining pressure ratio, reaching up to five times the initial compressive strength. The tensile and shear strengths, however, exhibit non-monotonic behaviour as the confining pressure ratio increases. At higher confining pressure ratio, both the tensile and shear strengths decrease, which shows agreement with the phenomenon observed by Sherman [1] in ballistic experiments that more tensile cracks were detected on the backside of the ceramic. In addition, the maximum radial confining pressure corresponds to the point where the tensile strength decreases to zero. This is consistent with the physical meaning of this parameter, that is, at this confining pressure, the ceramic can no longer resist normal loads.

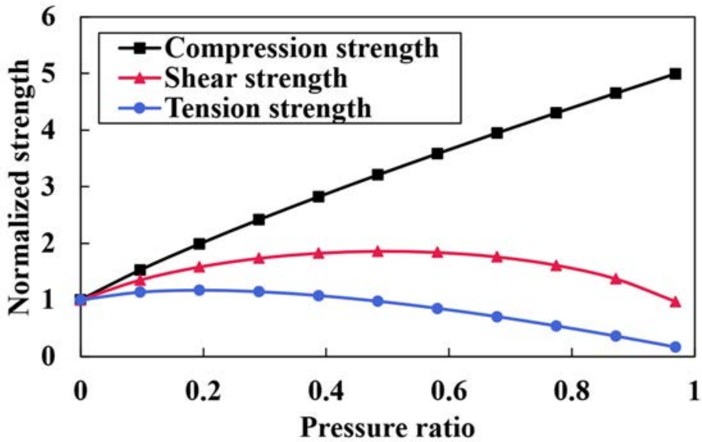

Figure 2: Variation of AD995 strength with confining pressure ratio.

2.2 Energy dissipation of composite armour system

Fig. 3 illustrates the penetration process for establishing the energy dissipation theory. During the penetration of the bi-layer composite armour, the projectile experiences mass loss and plastic deformation at the head. A crater forms on the surface of the ceramic due to crushing at first. Then, due to upward tensile cracks intersecting with the projectile head, a conical crack is formed [15].

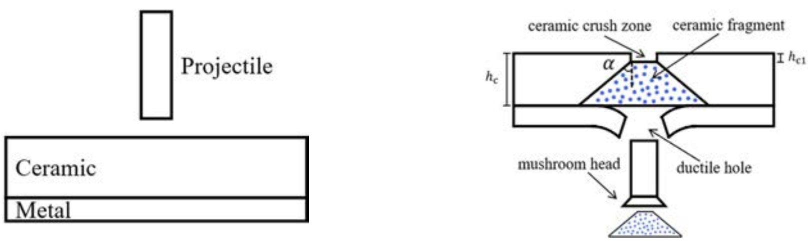

Figure 3: Schema of the penetration process. (a) Initial state; and (b) Terminal state.

2.2.1 Energy dissipation of projectile

The plastic deformation of the mushroom head has an established theoretical formula [16]. This formula can be used to calculate the length of the plastic zone and the plastic strain at each point. The plastic strain energy of the projectile can be calculated using eqn (3).

$$E_{\mathrm{p,d}} = \int_V \varepsilon_{\mathrm{p,d}} \sigma_{\mathrm{p}} dV. \tag{3}$$

- $E_{\mathrm{p,d}}$ is the plastic strain energy of the projectile.
- $\varepsilon_{\mathrm{p,d}}$ is plastic strain.
- σ_{p} is the yield strength of the projectile.

Eqn (4) serves to calculate the kinetic energy loss due to mass erosion. The key parameter $m_{\mathrm{p,e}}$ is difficult to determine using analytical methods. Eqn (5.1) determines three dimensionless variables affecting the erosion mass through dimensional analysis. Based on existing ballistic test results [8], [12], [17], the empirical expression for it is determined using symbolic regression, as shown in eqn (5.2).

$$E_{\mathrm{p,e}} = \frac{1}{2} m_{\mathrm{p,e}} v_{\mathrm{p}}^2. \tag{4}$$

$$\frac{m_{\mathrm{p,e}}}{\rho_{\mathrm{p}} d_{\mathrm{p}}^3} = f\left(\frac{\sigma_{\mathrm{c,c}}}{Y_{\mathrm{p}}}, \frac{h_{\mathrm{c}}}{d_{\mathrm{p}}}, \frac{v_{\mathrm{p}}}{\sqrt{Y_{\mathrm{p}}/\rho_{\mathrm{p}}}}\right), \tag{5.1}$$

$$\frac{m_{\mathrm{p,e}}}{\rho_{\mathrm{p}} d_{\mathrm{p}}^3} = \delta \frac{\sigma_{\mathrm{c,c}} h_{\mathrm{c}} v_{\mathrm{p}}}{d_{\mathrm{p}} \sqrt{Y_{\mathrm{p}}^3/\rho_{\mathrm{p}}}}. \tag{5.2}$$

- $E_{\mathrm{p,e}}$ is the erosion kinematic energy.
- v_{p} is the initial velocity of the projectile.
- ρ_{p} is the density of the projectile.
- d_{p} is the projectile diameter.
- Y_{p} is the flow stress of the projectile that equals to $1.7\sigma_{\mathrm{p}}$.
- h_{c} is the thickness of the ceramic front plate.

The form of eqn (5.2) is similar to the equation used in Tang and Wen [11] for studying the ballistic performance of composite armour without confining pressure. Instead of using the σ_{HEL}, the present theory uses compressive strength for dimensionless normalization to reflect the contribution of confining pressure. Fig. 4 compares the validity of the two dimensionless normalizations. The ballistic experiments in Zhang et al. [12] were conducted with a confining pressure target, while those in Sanchez-Galvez [8] and Hou et al. [17] were based on targets without confining pressure. The results show the advantage of the present theory which reveals the different erosion mass by ceramics with the same σ_{HEL} but different compressive strength.

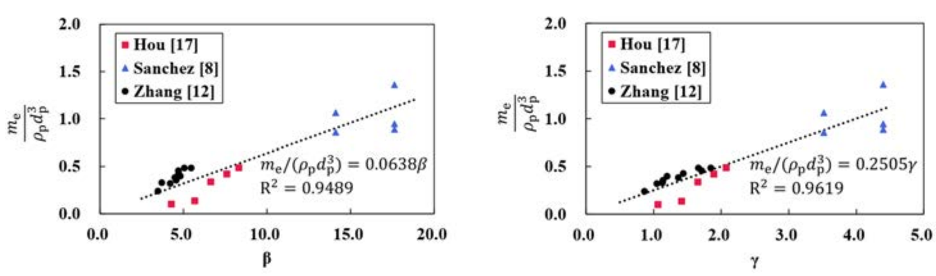

(a) (b)

Figure 4: Normalized erosion mass of projectiles. (a) The abscissa is normalized by σ_{HEL}; and (b) The abscissa is normalized by $\sigma_{\mathrm{c,c}}$.

The energy dissipation of the projectile is given by eqn (6).

$$E_{\mathrm{p}} = E_{\mathrm{p,e}} + E_{\mathrm{p,d}}. \tag{6}$$

2.2.2 Energy dissipation of ceramic front plate

The energy dissipation in the ceramic front plate can be divided into the crushing part and the shear part. The key parameter for the calculation is the height h_{c1} shown in Fig. 3(b). The following assumptions are adopted: (1) The conical crack is caused by the intersection of upward tensile cracks with the projectile head [15]; and (2) The propagation speed of the tensile cracks is 1/5 of the ceramic stress wave velocity [18]. Based on these assumptions, h_{c1} can be calculated using eqn (7).

$$\frac{h_{\mathrm{c1}}}{h_{\mathrm{c}}} = \frac{6u}{5u+c_{\mathrm{c}}}. \tag{7}$$

- u is the penetration velocity, $u = 0.15v_{\mathrm{p}}$ for steel projectile and $u = 0.4v_{\mathrm{p}}$ for tungsten alloy projectile [11].
- c_{c} is the ceramic stress wave velocity.

The crushing energy and the shear fracture energy are given by eqn (8) and eqn (9), respectively.

$$E_{\mathrm{c,c}} = \frac{\pi d_{\mathrm{p}}^2}{4} h_{\mathrm{c1}}\sigma_{\mathrm{c,c}}, \tag{8}$$

$$E_{\mathrm{c,s}} = \tau_{\mathrm{c,s}}\pi\left(d_{\mathrm{p}} + (h_{\mathrm{c}} - h_{\mathrm{c1}})\tan\alpha\right)\left(\frac{h_{\mathrm{c}}-h_{\mathrm{c1}}}{\cos\alpha}\right)\Delta_{\mathrm{c}}, \tag{9.1}$$

$$\Delta_{\mathrm{c}} = \gamma_{\mathrm{c}}\frac{h_{\mathrm{c}}-h_{\mathrm{c1}}}{\cos\alpha}. \tag{9.2}$$

- α is the half angle of ceramic cone.
- Δ_{c} is the fracture displacement along the crack direction which is corresponded to the ductility coefficient γ_{c} and the length of the crack.

Based on existing research results [9], [10], [19], the half-cone angle α under impact loading is 53°. The method for determining γ_{c} is given in Section 4.1.

Hence the total energy dissipated by the ceramic can be written as eqn (10).

$$E_{\mathrm{c}} = E_{\mathrm{c,c}} + E_{\mathrm{c,s}}. \tag{10}$$

2.2.3 Energy dissipation of metal back plate

The failure modes of the thin metal backing plate in composite armour can be classified into ductile hole failure and punching failure. This is primarily determined by the velocity of the projectile and the fractured ceramic cone. According to the ballistic experiments in Zhang et al. [12], within the velocity range studied in present paper, the failure mode of the backing plate is ductile hole failure. The energy dissipation formula can be given by the equation proposed by Woodward and Cimpoeru [20] as shown in eqn (11).

$$E_{\mathrm{m}} = \frac{\pi d_{\mathrm{p}}\sigma_{\mathrm{m}}h_{\mathrm{m}}(r_{\mathrm{p}}+\pi h_{\mathrm{m}})}{4}. \tag{11}$$

- σ_{m} is the tensile strength of the back plate.
- h_{m} is the thickness of the back plate.

In summary, the ballistic performance of the composite armour considering the effect of confining pressure can be expressed by eqn (12).

$$v_{\mathrm{res}} = \sqrt{\frac{m_{\mathrm{p}} v_{\mathrm{p}}^2 - 2(E_{\mathrm{p}} + E_{\mathrm{c}} + E_{\mathrm{m}})}{m_{\mathrm{p,res}} + m_{\mathrm{c,res}}}}, \tag{12.1}$$

$$m_{\mathrm{p,res}} = m_{\mathrm{p}} - m_{\mathrm{p,e}}, \tag{12.2}$$

$$m_{\mathrm{c,res}} = \frac{1}{3}\rho_{\mathrm{c}}\pi(h_{\mathrm{c}} - h_{\mathrm{c1}})\left(r_{\mathrm{top}}^2 + r_{\mathrm{top}}r_{\mathrm{bot}} + r_{\mathrm{bot}}^2\right), \tag{12.3}$$

$$r_{\mathrm{top}} = r_{\mathrm{p}},\ r_{\mathrm{bot}} = r_{\mathrm{p}} + \tan\alpha\,(h_{\mathrm{c}} - h_{\mathrm{c1}}). \tag{12.4}$$

- v_{res} is the residual velocity.
- $m_{\mathrm{c,res}}$ and $m_{\mathrm{p,res}}$ are the mass of the ceramic cone and the residual projectile respectively.

3 RESULTS AND DISCUSSIONS

3.1 Comparison between test and analytical model

Each determined confining pressure state corresponds to a specific ductility coefficient γ_{c}. According to the theory in Section 2, a ballistic performance prediction curve can be obtained. Based on the ballistic performance tests in Zhang [12], the data sets for three different confining pressures (0, 125 MPa, 274 MPa) are predicted through the present theory. The ductility coefficient for each curve is calculated by the principle of minimizing squared residuals.

Fig. 5 shows the optimal ballistic performance prediction curve and the corresponding ductility coefficient γ_{c}. Fig. 6 indicates that for AD995 ceramics, when the confining pressure ratio is less than 10%, the ductility coefficient exhibits a highly linear relationship with the confining pressure ratio. Table 1 presents a comparison between the prediction for the ballistic limit velocity in this paper and test data, demonstrating that the theory proposed in this paper also shows high accuracy in predicting the ballistic limit velocity.

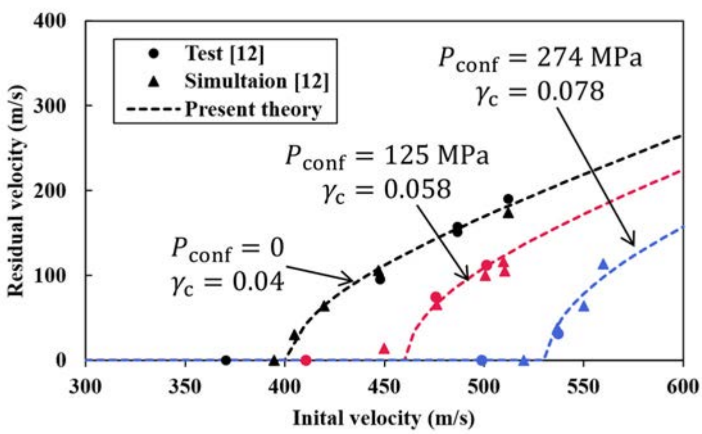

Figure 5: Prediction of ballistic performance with experiments and simulations.

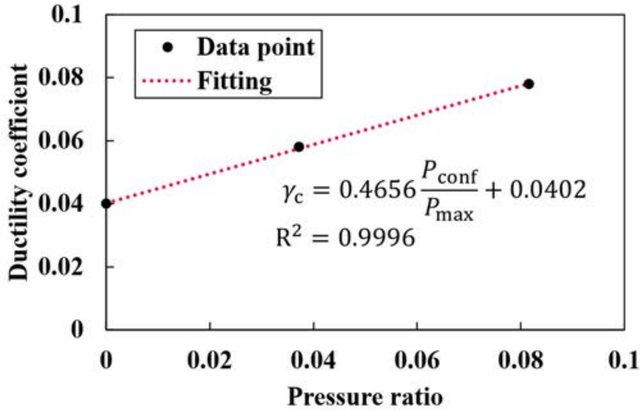

Figure 6: Fitting curve of ductility coefficient and confining pressure ratio.

Table 1: Ballistic limit velocity under confining pressure test.

P_{conf} (MPa)	h_c (mm)	h_m (mm)	Test BLV ($m{\cdot}s^{-1}$) [12]	Cal BLV ($m{\cdot}s^{-1}$)	Error (%)
0	6	3	398	400	1.8
125	6	3	440	465	5.7
274	6	3	499–537	530	−1.3 to 6.2

3.2 Contribution of strength and ductility in analytic model

This paper introduces two improvements compared to existing theories: the enhancement of ceramic strength and ductility under confining pressure. To verify the significance of improvements, contribution coefficient analyses for both strength enhancement and ductility enhancement are conducted.

Eqn (13) and eqn (14) are defined for contribution coefficient of strength and ductility, respectively.

$$\delta_D|_{P_{conf}} = \left(\frac{1}{n}\sum_{i=1}^{n}\frac{1}{|\gamma_{c,0}-\gamma_{c,i}|}\frac{\int_0^{v_{p,max}}|v_{res,0}-v_{res,i}|dv}{\int_0^{v_{p,max}}v_{res,0}dv}\right)\Bigg|_{P_{conf}}, \quad (13)$$

$$\delta_S|_{P_{conf}} = \left(\frac{\int_0^{v_{p,max}}\left|v_{res,P_{conf}}-v_{res,P_{conf}=0}\right|dv}{\int_0^{v_{p,max}}v_{res,P_{conf}}dv}\right)\Bigg|_{P_{conf}}. \quad (14)$$

The contributions of strength and ductility enhancement are measured by the ratio of the area difference enclosed by the curves and the absolute value of the parameter changes. The range of the contribution coefficient is $[0, +\infty)$. A larger contribution coefficient indicates the higher significance in the ballistic performance calculation.

Fig. 7 and Table 2 show the ductility and strength contribution coefficients for different target configurations. The results indicate that the contribution coefficients increase with the rise of the pressure ratio. This suggests that the two correction parameters proposed in this paper are essential for the ballistic performance calculation of composite armour under confining pressure. Furthermore, these two coefficients are numerically close, revealing that the importance of these two corrections for the theoretical calculation is consistent. Removing either parameter would lead to deviations for the results.

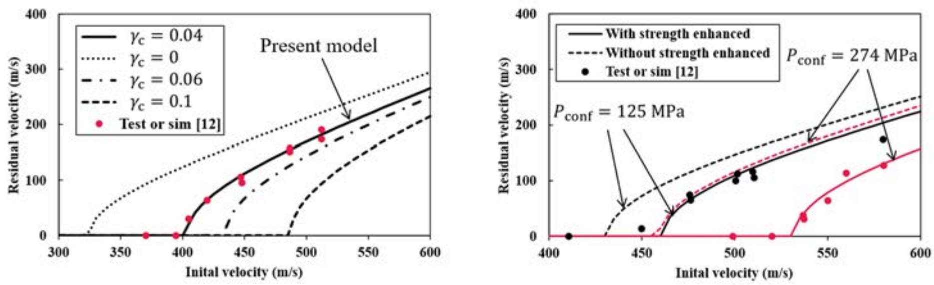

(a) (b)

Figure 7: Contribution of ductility and strength. (a) Results with different ductile coefficient γ_c for $P_{conf} = 0$; and (b) Results with and without strength enhanced.

Table 2: Contribution coefficient of ductility and strength.

Contribution coefficient	P_{conf} **(MPa)**	**Pressure ratio (%)**	δ_D **or** δ_S
Ductility	0	0	0.106
	125	3.72	0.197
	274	8.15	0.355
Strength	125	3.72	0.101
	274	8.15	0.293

3.3 Applicability of the analytic model

To verify the applicability of the theory proposed in this paper, this section selects ballistic experiments involving different projectiles penetrating various configurations of bi-layer ceramic/metal composite armour. The tensile strengths σ_m of 2024-T3 and GFRP are 600 MPa [21] and 1000 MPa [22], respectively. The yield strength σ_p of the 4340 steel projectile is 785 MPa [12], and the key JH-2 parameters for the ceramics are provided in Table 3.

Table 3: JH-2 parameters of AD995, AD95 and AD85.

Ceramic	ρ_c **(kg·m^{-3})**	σ_{HEL} **(GPa)**	P_{HEL} **(GPa)**	**A**	**N**
AD995 [12]	3890	6.54	3.51	0.88	0.64
AD95 [23]	3750	6.0	3.2	0.889	0.764
AD85 [24]	3480	2.0	1.46	0.93	0.6

Table 4 demonstrates the applicability of the theory proposed in this paper. Additionally, for conditions with higher projectile velocities, the predicted residual velocity is lower. This is mainly due to two reasons: (1) Under high-speed penetration, the failure mode of the backing metal transitions from ductile hole failure to adiabatic shear failure that dissipates less energy during the penetration process; and (2) The fracture ceramic will not form a complete ceramic cone moving together with the projectile, meaning the actual ceramic mass $m_{c,res}$ will be lower than the predicted.

Table 4: Ballistic performance prediction accuracy under different armour configurations.

Armour configuration	h_c (mm)	h_m (mm)	v_p (m·s^{-1})	$v_{res,exp}$ (m·s^{-1})	$v_{res,cal}$ (m·s^{-1})	**Error (%)**
Projectile: 4340 steel $\phi 7.62 \times 20$ Target: AD995+2024T3 [12]	6	3	447	96	107	11.9
	6	3	486	152	154	1.4
	6	3	512	191	181	−5.0
	6	3	476	75	68	−9.6
	6	3	501	112	111	−0.6
Projectile: 4340 steel $\phi 7.56 \times 30.5$ Target: AD95+2024T3 [23]	6.1	6	650	341	330	−3.3
	6.12	6	655	351	335	−4.7
	6.14	6.03	830	559	515	−7.8
	6.1	5.87	712	430	400	−7.0
	8.96	6	775	370	359	−3.0
	8.98	5.97	845	463	419	−9.5
	6.14	6.88	860	580	527	−9.2
Projectile: 4340 steel $\phi 12.7 \times 45$ Target: AD85+GFRP [22]	4	5	893	832	722	−13.2
	6	5	880	800	678	−15.2
	9	5	898	693	636	−8.2
	9	8	880	658	575	−12.7
	9	10	882	621	535	−13.9
	18	5	895	425	402	−5.4
	18	8	888	329	359	9.1
	18	10	876	299	311	3.9

4 CONCLUSIONS

This paper proposes a ballistic performance calculation method that considers the enhancing effect of confining pressure on ceramics based on the energy dissipation principle. The theoretical prediction results are in good agreement with various ballistic experiments. The main conclusions are as follows:

1. The present theory can predict the ballistic performance of targets with a confining pressure ratio below 10% (including no confining pressure). When the initial speed is below 850 m/s, the prediction error is within 10% compared to the experiments. For projectile speed exceeding 850 m/s, the prediction error remains within 15%.
2. The two theoretical improvements introduced which are the ductility coefficient of ceramic and the enhancement of ceramic strength due to confining pressure, both contribute equally to the increment of the theory accuracy. The degree of improvement increases with the rise of confining pressure ratio.

ACKNOWLEDGEMENTS

This research was supported by the National Natural Science Foundation of China (Grant No. 52278526) and the Natural Science Foundation of Shanghai (Grant No. 22dz1202900).

REFERENCES

[1] Sherman, D., Impact failure mechanisms in alumina tiles on finite thickness support and the effect of confinement. *International Journal of Impact Engineering*, **24**(3), pp. 313–328, 2000.
[2] Holmquist, T.J. & Johnson, G.R., Modeling prestressed ceramic and its effect on ballistic performance. *International Journal of Impact Engineering*, **31**(2), pp. 113–127, 2005.
[3] Farbaniec, L. et al., Damage evolution of hot-pressed boron carbide under confined dynamic compression. *International Journal of Impact Engineering*, **99**, pp. 75–84, 2017.
[4] Chi, R. et al., Pre-stress effect on confined ceramic armor ballistic performance. *International Journal of Impact Engineering*, **84**, pp. 159–170, 2015.
[5] Lundberg, P., Renström, R. & Andersson, O., Influence of confining prestress on the transition from interface defeat to penetration in ceramic targets. *Defence Technology*, **12**(3), pp. 263–271, 2016.
[6] Xu, W. et al., Effects of dynamic prestress on silicon carbide ceramic against long rod impact. *Journal of Physics: Conference Series*, **2478**(7), 2023.
[7] Florence, A.L., Interaction of Projectiles and Composite Armour Part II. Report, Defense Technical Information Center, USA, 1969.
[8] Sanchez-Galvez, V., Impact behaviour of lightweight armours. *WIT Transactions on The Built Environment*, vol. 25, WIT Press: Southampton and Boston, pp. 91–101, 1970.
[9] Woodward, R.L., A simple one-dimensional approach to modelling ceramic composite armour defeat. *International Journal of Impact Engineering*, **9**(4), pp. 455–474, 1990.
[10] Feli, S., Aalami-Aaleagha, M.E. & Ahmadi, Z., A new analytical model of normal penetration of projectiles into the light-weight ceramic-metal targets. *International Journal of Impact Engineering*, **37**(5), pp. 561–567, 2010.
[11] Tang, R.T. & Wen, H.M., Predicting the perforation of ceramic-faced light armors subjected to projectile impact. *International Journal of Impact Engineering*, **102**, pp. 55–61, 2017.
[12] Zhang, R. et al., Influence of prestress on ballistic performance of bi-layer ceramic composite armors: Experiments and simulations. *Composite Structures*, **227**, 2019.
[13] Zhang, R., Han, B. & Lu, T.J., Confinement effects on compressive and ballistic performance of ceramics: A review. *International Materials Reviews*, **66**(5), pp. 287–312, 2020.
[14] Johnson, G.R. & Holmquist, T.J., Response of boron carbide subjected to large strains, high strain rates, and high pressures. *Journal of Applied Physics*, **85**(12), pp. 8060–8073, 1999.
[15] Zaera, R. & Sanchez-Galvez, V., Analytical modelling of normal and oblique ballistic impact on ceramic/metal lightweight armours. *International Journal of Impact Engineering*, **21**(3), pp. 133–148, 1998.
[16] Taylor, G., The use of flat-ended projectiles for determining dynamic yield stress I: Theoretical considerations. *Proceedings of the Royal Society of London Series A Mathematical and Physical Sciences*, **194**(1038) pp. 289–299, 1948.
[17] Hou, H.L., Zhu, X. & Li, W., Investigation on bullet proof mechanism of light ceramic/steel composite armor. *Acta Armamentarii*, **34**(1), pp. 105–114, 2013. (In Chinese.)
[18] Reijer, P.C.D., Impact on ceramic faced armour. Doctoral thesis, TU Delft, The Netherlands, 1991.

[19] Wilkins M.L., Fourth Progress Report of Light Armor Program. Technical Report, U.S. Department of Energy Office of Scientific and Technical Information, USA, 1969.
[20] Woodward, R.L. & Cimpoeru, S.J., A study of the perforation of aluminium laminate targets. *International Journal of Impact Engineering*, **21**(3), pp. 117–131, 1998.
[21] Abotula, S. & Chalivendra, V.B., An experimental and numerical investigation of the static and dynamic constitutive behaviour of aluminium alloys. *The Journal of Strain Analysis for Engineering Design*, **45**(8), pp. 555–565, 2010.
[22] Hetherington, J.G. & Rajagopalan, B.P., An investigation into the energy absorbed during ballistic perforation of composite armours. *International Journal of Impact Engineering*, **11**(1), pp. 33–40, 1991.
[23] Serjouei, A. et al., Experimental validation of BLV model on bi-layer ceramic-metal armor. *International Journal of Impact Engineering*, **77**, pp. 30–41, 2015.
[24] Ma, G. & Wang, F., Modeling the confinement and prestress effects on dynamic failure of ceramic deep beam. *International Journal of Protective Structures*, **4**(2), pp. 189–207, 2013.